

A generalized control scheme for system uncertainty estimation and cancellation

Transactions of the Institute of

Measurement and Control

2021, Vol. 43(13) 2921–2933

© The Author(s) 2021

Article reuse guidelines:

sagepub.com/journals-permissions

DOI: 10.1177/01423312211010509

journals.sagepub.com/home/tim



Qing-Guo Wang¹, Tao Liu², Zhuo-Yun Nie³ , Shoulin Hao², Xuhui Ren²,
Dan Zhang⁴  and Lei Wang⁵

Abstract

This paper addresses the control of a continuous-time system with possibly large uncertainty of unknown internal dynamics or external disturbance. A novel control scheme is proposed to estimate and cancel the system uncertainty effectively so as to enhance disturbance rejection (DR) performance. Unlike asymptotic analysis with infinite gain in the literature, the estimation transient analysis is carried out for the proposed scheme with a finite estimator gain and the precise error formulas are derived, based on a classical low-order plant description. The control performance associated with a realizable gain is quantified by tight bounds with respect to the ideal case, which enables easy parameter tuning. The necessary and sufficient condition for the internal stability of the control system is established, along with a D-decomposition method for determining the complete set of the gain intervals that could internally stabilize the plant. In the presence of measurement noise, a low-pass filter is introduced to attenuate its adverse effect. Simulations and semi-realistic experiments are performed to demonstrate the effectiveness of the proposed scheme, which shows evident improvement on DR performance over the well-known active DR control.

Keywords

Uncertain systems, robust control, disturbance rejection, extended state observer, internal stability

Introduction

Without loss of generality but for simplicity of exposition, let us consider a plant described by a second-order model, as given by Equation (1):

$$\ddot{y} = f(\dot{y}, y, u, w) + b_0 u, \quad (1)$$

where u , y and w are the system input, output and external disturbance, respectively; $f(\dot{y}, y, u, w)$ represents the total system uncertainty including the unknown and probably time-varying system dynamics and external disturbance; and b_0 is the nominal input gain. Over a long history, researchers in the control field have been attempting different ways to estimate f and then cancel it with the control action, such that the resulting system becomes simple and linear for control design. With the estimation and compensation for f , some standard linear feedback control schemes can be applied to meet the desired closed-loop target, which gives the dynamic feedback linearization in a unified framework.

The active disturbance rejection control (ADRC) (Gao, 2014; Han, 2009) and the disturbance-observer based control (DOBC) (Chen et al., 2016) are developed for effective disturbance rejection (DR) control. These methods can be implemented in the industry applications due to the simple structure and capability in dealing with model uncertainties, nonlinearity and external disturbance within a unified framework. The recent success also includes piezoelectric actuators

(Nie et al., 2018) and the lithium-ion battery (Sun et al., 2020). Rather than using the complex nonlinearity functions or high gain technologies, adaptive technologies provide alternative means to improve the DR performance. The adaptive control (Astrom and Wittenmark, 1994) determines a parameterized model for f in real time and updates its control law according to the latest model, such that the closed-loop system could behave as desired with no or little change regardless of how f changes. In Wang et al. (2017), adaptive technology is used to adjust the controller gain as well as f to enhance the DR performance in the DR framework. To

¹Guangdong Key laboratory for Artificial Intelligence and Multi-Modal Data Processing, United International College (UIC), Beijing Normal University-Hong Kong Baptist University, China

²Institute of Advanced Control Technology, Dalian University of Technology, China

³School of Information Science and Engineering, National Huaqiao University, China

⁴Department of Automation, Zhejiang University of Technology, China

⁵School of Automation Science and Electrical Engineering, Beihang University, China

Corresponding author:

Zhuo-Yun Nie, School of Information Science and Engineering, National Huaqiao University, Xiamen, 361021, China.

Email: yezhuyun2004@sina.com

balance the DR and noise tolerance, the adaptive extended state observer (ESO) was developed in the framework of the ADRC scheme to deal with the uncertainties and measurement noise (Xue et al., 2015).

The neural control (Ge and Tee, 2006) trains an artificial neural network with a learning algorithm to approximate f in real time, after which the controller is designed similarly to the above principle. Under an adaptive robust control framework, a neural network is designed as an uncertainty compensator to approximate the compound disturbance (Sheng et al., 2021). In the ADRC control scheme, adaptive backpropagation neural networks are used as a feed-forward inverse controller for nonlinear function approximation (Liu et al., 2020). To produce a better convergence in both the estimation and tracking tasks, a differential neural network observer is used to produce a nonlinear approximation of the matched perturbation and the unknown states simultaneously in the transformed coordinates (Salgado et al., 2017). Note that the stability conditions of these methods were discussed under various assumptions, which motivates us to investigate rigorous design and analysis in the DR framework.

It deserves particular attention that in the past decade, there have emerged new control approaches based on ESO for delay-free (Chen et al., 2013; Guo and Zhao, 2011b, 2012; Huang and Xue, 2014; Li et al., 2016; Sun et al., 2016; Zhao and Guo, 2017; Zheng et al., 2012) or time-delay (Hao et al., 2017; Liu et al., 2017) systems, and many application studies have appeared (Li et al., 2012; Liu and Li, 2011; Mao et al., 2018; Wang et al., 2015; Yao et al., 2014) as well. The ESO regards f as an extended state variable and exploits the standard observer theory to estimate the extended state including the original system state and the above variable. This scheme is simple to understand and implement while it has the potential to work against a larger class of uncertainty f than other schemes mentioned above. However, the dynamics of the state estimation error for ESO are not homogeneous but admit the additional input term related to f , which is further coupled with this error. Unlike the standard state observer for which the estimation error goes to zero asymptotically with a finite observer gain, asymptotic estimation of f with ESO could be achieved only when very restrictive assumptions on f are imposed. The observer gain must be infinity (Zhao and Guo, 2017), and a square wave of disturbance may fail these assumptions. More critically, due to the fact that f is a function of the plant state which is included in the extended state to be estimated, any assumption on f could provoke a circular argument in logic and therefore, should be avoided for technical rigour and practical applicability. To our best knowledge, there is no study which shows a precise relationship between a finite observer gain and the transient performance of the state estimation or plant output. The design of ESO and the related controller are still left to trial and error or artificial tuning rules.

In this paper, a novel control scheme is proposed for the system uncertainty estimation and cancellation with differentiators, which have the salient features: (a) \ddot{y} instead of f is estimated such that f can be simply obtained from Equation (1) as $f = \ddot{y} - b_0 u$, considering that \ddot{y} is obviously related to y and such a relation is independent of any f and u . This enables us to establish a simple, direct and fixed relationship

between \ddot{y} and its estimate, and so is for f and its estimate. As a result, asymptotic estimation of f is achieved without any assumption on f and u ; and (b) the above relations enable a simple yet precise tuning of the finite estimator gain given a specified estimation error tolerance. For practical application, an approximate differentiator is adopted to estimate the output derivatives. The contributions of this paper are highlighted as follows:

- (a) a new DR control scheme is proposed for a linear or nonlinear system with possibly large uncertainty consisting of unknown internal dynamics or external disturbance;
- (b) rigorous analysis of the system with a finite gain, which is not addressed in the literature of ESO, is presented. Particularly, the estimation transient is analysed for the proposed scheme with a finite estimator gain and precise error formulae are obtained; and
- (c) the necessary and sufficient condition for the internal stability of the control system is established, along with a D-decomposition method to determine the complete set of the internally stabilized gain intervals.

In the rest of the paper, the proposed control scheme is presented in the second section. Performance analysis is given in the third section while stability analysis is addressed in the fourth section. The fifth section shows the simulation and experimental results. The sixth section concludes the paper.

Proposed control scheme

The proposed control scheme is shown in Figure 1, consisting of two loops. The inner one is to estimate and cancel the system uncertainty f , while the outer loop is to control the resulting integral plant with state feedback for a desired closed-loop performance. Note that $L_f(s)$ is a low-pass filter which is used for noise attenuation and therefore, and this will be discussed solely in the fifth section where the measurement noise $n(t)$ is considered in simulation and experiment. Hence, $n(t) = 0$ and $L_f(s) = 1$ are assumed in other sections concerned with internal stability and estimation of the control performance.

Based on the plant model in Figure 1, once the differential signal $\hat{\ddot{y}}$ is found in the inner loop, the total uncertainty, $f(\hat{y}, y, u, w)$, is obtained directly as $\hat{f} = \hat{\ddot{y}} - b_0 u$. A simple controller for the inner loop, as given by Equation (2):

$$u = \frac{-\hat{f} + u_0}{b_0}, \quad (2)$$

reduces the system to Equation (3):

$$\ddot{y} \approx u_0, \quad (3)$$

for which any linear control design method such as a proportional–integral–derivative (PID) controller (Wang et al., 1999a), linear–quadratic regulator controller (He et al., 2000), and pole placement (Zhang et al., 2002) can be well adopted. As a result, a simple choice of the outer loop controller could be linear state feedback, as given by Equation (4):

$$u_0 = \alpha_0 r - \alpha_1 \hat{y} - \alpha_0 y, \quad (4)$$

which, in view of Equation (3), approximately achieves the following overall closed-loop transfer function from the reference r to the output y , as given by Equation (5):

$$G_{yr}(s) = \frac{\alpha_0}{s^2 + \alpha_1 s + \alpha_0}, \quad (5)$$

where two parameters are selected to meet the desired performance specifications with the desired closed-loop characteristic polynomial, as given by Equation (6):

$$\alpha(s) \triangleq s^2 + \alpha_1 s + \alpha_0. \quad (6)$$

Obviously, a key issue of the proposed control scheme lies with the design of the inner loop, that is, how well \ddot{y} can be estimated, given only the measured $y(t)$. Note that the Laplace transform of $\dot{y}(t)$ under a zero initial condition is $sy(s)$. But the ideal differential operator, $D(s) = s$, is not proper and thus cannot be realized physically. It is therefore replaced by the following practical differential operator, as given by Equation (8):

$$D(s) = \frac{sk}{s+k}, \quad (7)$$

so that we obtain Equation (8):

$$\hat{\dot{y}}(s) = D(s)y(s), \quad (8)$$

Where a positive constant is k . Similarly, the second derivative of $y(t)$ is estimated as given by Equation (9):

$$\hat{\ddot{y}}(s) = D^2(s)y(s). \quad (9)$$

Thus, \ddot{y} and its estimate are related to each other via Equations (10) and (11):

$$\hat{\ddot{y}}(s) = Q_2(s)\ddot{y}(s), \quad (10)$$

where:

$$Q(s) = \frac{k}{s+k}, \quad Q_2(s) = Q^2(s). \quad (11)$$

It follows from Equations (10) and (11) that $\hat{\ddot{y}}(s) = \ddot{y}(s)$ when k tends to infinity, regardless of f and u . In fact, it is seen from Equation (10) that $\hat{\ddot{y}}$ is not always equal to \ddot{y} . Using u directly in $\hat{f} = \hat{\ddot{y}} - b_0 u$ with $H = 1$ will therefore not give exactly $\hat{f} = f$. Besides, using u directly in Figure 1 with $H = 1$ will lead to an algebraic loop that may cause a problem for implementation. To tackle the problem, the input filter H is chosen as given by Equation (12):

$$H(s) = Q_2(s) = \left(\frac{k}{s+k} \right)^2. \quad (12)$$

It follows from Figure 1 and Equation (10) that we obtain Equation (13):

$$\hat{f}(s) = Q_2(s)\ddot{y}(s) - Q_2(s)b_0 u(s) = Q_2(s)f(s). \quad (13)$$

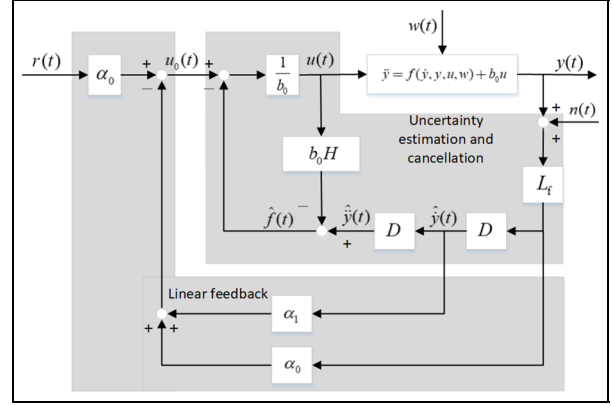


Figure 1. Proposed control scheme.

which exactly inherits the same relationship between \ddot{y} and $\hat{\ddot{y}}$ in Equation (10). Hence, the estimation error for f goes to zero when k tends to infinity, regardless of f and u .

Remark 1: As discussed by Han (2009), the commonly used tracking differentiator and ESO can be viewed as a differential estimator to observe the derivative of the system output. Although their convergence has been well studied (Guo and Zhao, 2011a, 2011b, 2012), these two methods often involve additional phase lag in the estimation. The proposed differential operator $D(s)$ in Equation (7) gives a simple but practical manner to realize differential estimation. In fact, our scheme can be simply implemented by the existing technologies. Note that the proposed D -controller is available in industrial controller products. It approximates the differential operator and has been widely used in commercial PID controllers for implementing the derivative action. One can simply cascade a number of such D -term in place of $D(s)$ in Figure 1, tune the parameter k based on practical requirements, and finally set $H(s)$ in Figure 1 according to Equation (7) with the tuned k . The exact formula to tune k based on the time domain analysis is given in the next section.

Performance analysis

Consider now the estimation performance, that is, its error transient. Note that the transient solution for a signal in a linear system has a basic component of $e^{\lambda t}$, which can express a constant, sine, or general exponential function with a proper choice of λ . Thus, suppose $y(t) = e^{\lambda t}$. It follows from Equation (8) that we obtain Equation (14):

$$\hat{\dot{y}}(s) = \frac{sk}{s+k} \frac{1}{s-\lambda}. \quad (14)$$

whose inverse Laplace transform is given by Equation (15):

$$\hat{\dot{y}}(t) = \frac{k}{k+\lambda} (ke^{-kt} + \lambda e^{\lambda t}). \quad (15)$$

Note that the exact derivative is given by $\dot{y}(t) = \lambda e^{\lambda t}$. The relative estimation error for $\dot{y}(t)$ is then obtained as given by Equation (16):

$$e_1(t, k) \triangleq \left| \frac{\dot{y}(t) - \hat{\dot{y}}(t)}{\dot{y}(t)} \right| = \left| \frac{\lambda}{k + \lambda} - \frac{k^2}{(k + \lambda)\lambda} e^{-(k + \lambda)t} \right|, \lambda \neq 0. \quad (16)$$

One sees that

$$\lim_{k \rightarrow \infty} e_1(t, k) = 0, \forall t, |\lambda| \in (0, \infty).$$

Similarly, it follows from Equation (9) that

$$\hat{\dot{y}}(s) = \left(\frac{sk}{s + k} \right)^2 \frac{1}{s - \lambda},$$

whose inverse Laplace transform is given by

$$\begin{aligned} \hat{\dot{y}}(t) = L^{-1}[\hat{\dot{y}}(s)] &= \frac{(k^4 + 2\lambda k^3)}{(k + \lambda)^2} e^{-kt} \\ &+ \frac{k^2 \lambda^2}{(k + \lambda)^2} e^{\lambda t} - \frac{k^4 t}{(k + \lambda)} e^{-kt}. \end{aligned}$$

Since $\ddot{y}(t) = \lambda^2 e^{\lambda t}$, a relative estimation error for $\ddot{y}(t)$ is then obtained as given by Equation (17):

$$\begin{aligned} e_2(t, k) &\triangleq \left| \frac{\ddot{y}(t) - \hat{\ddot{y}}(t)}{\ddot{y}(t)} \right| \\ &= \left| \frac{2k\lambda + \lambda^2}{(k + \lambda)^2} - \frac{(k^4 + 2\lambda k^3)}{(k + \lambda)^2 \lambda^2} e^{-(k + \lambda)t} + \frac{k^4}{(k + \lambda)\lambda^2} t e^{-(k + \lambda)t} \right|, \\ &\lambda \neq 0. \end{aligned} \quad (17)$$

It is once again seen that

$$e_2(t) \triangleq \lim_{k \rightarrow \infty} e_2(t, k) = 0, \forall t, |\lambda| \in (0, \infty).$$

It should be stressed that the formula in Equation (17) gives a precise estimation error transient rather than a loose error bound. Hence, it is convenient to tune k with regard to a specified error tolerance such as given by Equation (18):

$$e_2(k) \triangleq \lim_{k \rightarrow \infty} e_2(t, k) = \frac{2k\lambda + \lambda^2}{(k + \lambda)^2}. \quad (18)$$

For example, letting $\lambda = 1$ and $e_2(\infty, k) = \frac{2k + 1}{(k + 1)^2} \leq 10\%$ yields $k \geq 18.5$. The general relationship between e_2 and k is depicted in Figure 2.

To address the control performance, suppose that the uncertainty in Figure 1 is linear, $f(\dot{y}, y, u, w) = -a_1 \dot{y} - a_0 y + w$, which implies that the plant is equivalently described by its transfer function model,

$$y(s) = G(s)[u(s) + w(s)] = \frac{b_0}{s^2 + a_1 s + a_0} [u(s) + w(s)].$$

By viewing Figure 1 as a signal flow graph with $n(t) = 0$ and $L_f(s) = 1$, Mason's formula (Franklin et al., 2014) is invoked to find the transfer function from a signal z_1 to another z_2 as given by Equation (19):

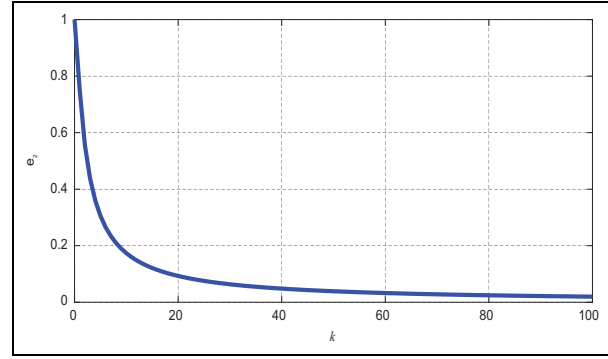


Figure 2. The relationship between e_2 and k .

$$G_{21} = \frac{z_2(s)}{z_1(s)} = \frac{1}{\Delta} \sum_i (G_i \Delta_i), \quad (19)$$

where G_i is the gain (transfer function) of the i -th forward path from z_1 to z_2 ; Δ is the system determinant defined as given by Equation (20):

$$\Delta = 1 - \sum_i (F_{1i}) + \sum_j (F_{2j}) - \sum_k (F_{3k}) + \dots \quad (20)$$

F_{1i} are the loop gains, F_{2i} are the products of 2 non-touching loop gains, F_{3i} are products of 3 non-touching loop gains, and Δ_i is the system determinant when the i -th forward path is removed from the system. It is readily seen from Figure 1 that there are four loops counted from the most inner one to the most outer with their loop gains being $H(s)$, $-G(s)D(s)D(s)/b_0$, $-\alpha_1 G(s)D(s)/b_0$ and $-\alpha_0 G(s)/b_0$, respectively. All the four loops share the common path from u_0 to u so that they are all touched and there are no non-touching loops. Thus, the system determinant is obtained as given by Equation (21):

$$\begin{aligned} \Delta &= 1 - H(s) + \frac{G(s)D(s)D(s)}{b_0} + \frac{\alpha_1 G(s)D(s)}{b_0} + \frac{\alpha_0 G(s)}{b_0} \\ &= 1 - \frac{k^2}{(s + k)^2} + \frac{k^2 s^2}{a(s)(s + k)^2} + \frac{\alpha_1 k s}{a(s)(s + k)} + \frac{\alpha_0}{a(s)}. \end{aligned} \quad (21)$$

where $a(s) = s^2 + a_1 s + a_0$ is the monic denominator of $G(s)$.

Consider the output in response to the setpoint r . Obviously, one has

$$\sum_i (G_i \Delta_i) = \alpha_0 / a(s).$$

Thus, from r to y the (closed-loop) transfer function is as given by Equation (22):

$$\begin{aligned} G_{yr}(s) &= \frac{\alpha_0 / a(s)}{1 - \frac{k^2}{(s + k)^2} + \frac{k^2 s^2}{a(s)(s + k)^2} + \frac{\alpha_1 k s}{a(s)(s + k)} + \frac{\alpha_0}{a(s)}} \\ &= \frac{\alpha_0 (s + k)^2}{a(s)s(s + 2k) + k^2 s^2 + \alpha_1 k s(s + k) + \alpha_0 (s + k)^2}. \end{aligned} \quad (22)$$

Its static gain is $G_{yr}(0) = 1$, indicating that the output y will track the set point r of step type asymptotically with no steady-state error if the transfer function is stable.

Similarly, one can obtain the transfer function from w to y as given by Equation (23):

$$G_{yw}(s) = \frac{b_0 s(s + 2k)}{a(s)s(s + 2k) + k^2 s^2 + \alpha_1 k s(s + k) + \alpha_0 (s + k)^2}. \quad (23)$$

Its static gain is $G_{yw}(0) = 0$, implying the system will reject a disturbance of step type asymptotically with no steady-state output error.

We now turn to transient performance. Let us first consider the limiting case of a very large k . Note that each block in Figure 1 has a finite frequency response over all frequencies even if the gain k tends to infinity, therefore different from high-gain control strategies in the literature. In fact, the loop transfer function viewed from the block of $(1/b_0)$ in Figure 1 as an equivalent single-loop feedback system is given by

$$L(s) = -\frac{k^2}{(s + k)^2} + \frac{k^2 s^2}{a(s)(s + k)^2} + \frac{\alpha_1 k s}{a(s)(s + k)} + \frac{\alpha_0}{a(s)},$$

which implies

$$\lim_{k \rightarrow \infty} L(s) = \frac{(\alpha_1 - a_1)s + (\alpha_0 - a_0)}{s^2 + a_1 s + a_0},$$

whose frequency response has limited magnitude and phase over all the frequencies. One sees from Equations (22) and (23) that the limiting closed-loop transfer functions from two external inputs are given, respectively, by Equations (24) and (25):

$$G_{yr}^\infty(s) \triangleq \lim_{k \rightarrow \infty} G_{yr}(s) = \frac{\alpha_0}{s^2 + \alpha_1 s + \alpha_0}, \quad (24)$$

$$G_{yw}^\infty(s) \triangleq \lim_{k \rightarrow \infty} G_{yw}(s) = 0, \quad (25)$$

for which the respective output transients in time domain can be easily determined and analysed without further discussion.

A challenging issue is to tune a finite k for practical implementation with a prescribed performance specification. Recall that in control engineering, the gain margin and bandwidth are often used to measure such a specification. When a finite gain of k is used rather than an infinite one, the performance will drop from the ideal case in Equation (24). Suppose that the degradation is assessed by a gain reduction ratio at a chosen frequency of ω_c (say, the desired bandwidth) such that we obtain Equation (26):

$$|G_{yr}(j\omega_c)| = \rho_g |G_{yr}^\infty(j\omega_c)|, \rho_g \in (0, 1). \quad (26)$$

Given a user-specified ρ_g , one can easily determine the corresponding k from Equation (26) as follows. The left-hand side of Equation (26) is a function of k , while the right-hand side of Equation (26) is a constant corresponding to a horizontal line against k . The intersections of these two plots meet

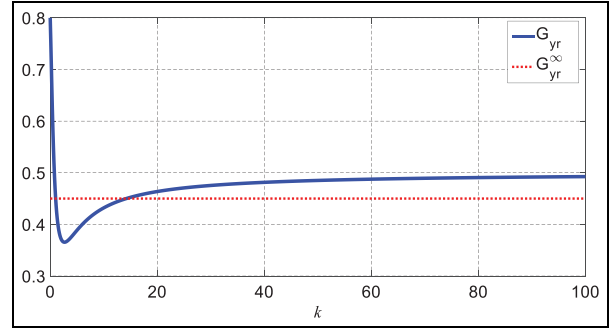


Figure 3. Tuning of k to meet the gain specification.

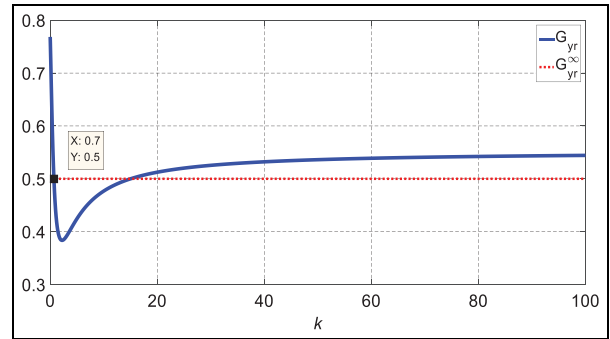


Figure 4. Tuning of k to meet the bandwidth specification.

Equation (26) and thus give solutions for k . For example, consider Equation (27):

$$G(s) = \frac{4}{s^2 + 2s + 3}. \quad (27)$$

Let $\omega_c = 2$ and $\rho_g = 0.9$. We obtain the solutions of Equation (26) for this example from Figure 3 as $k_1 = 1$ and $k_2 = 14.2$. $k_2 = 14.2$ is preferred because a larger gain ensures better estimation transient in general. This choice gives a smoother magnitude curve nearby (more robust against the model uncertainty) in view of Figure 3.

Alternatively, a finite gain of k will reduce the closed-loop bandwidth compared with the ideal one in Equation (24). Thus, suppose that the degradation is assessed by a bandwidth reduction ratio ρ_m such that we obtain Equation (28):

$$|G_{yr}(j\rho_m\omega_c)| = |G_{yr}^\infty(j\omega_c)|, \rho_m \in (0, 1). \quad (28)$$

Given a user-specified ρ_m , one can determine the corresponding k from Equation (28) in a similar way to that for Equation (26). Consider $G(s)$ in Equation (27) again. Let $\omega_c = 2$ and $\rho_m = 0.9$, so we obtain the solutions of Equation (28) for this example from Figure 4 as $k_1 = 0.7$ and $k_2 = 15.1$.

Consider the error between $G_{yr}(s)$ in Equation (22) and its limiting case in Equation (24). This error measures the performance loss with a finite gain k from the ideal case of the infinite gain. Define $E(\omega) = ||G_{yr}(j\omega)| - |G_{yr}^\infty(j\omega)||$. To assess the

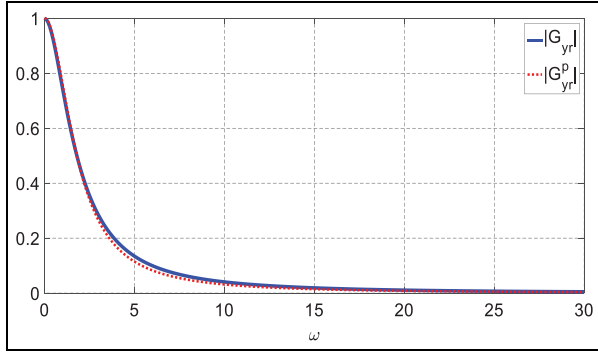


Figure 5. Plot of $|G_{yr}(j\omega)|$ and $|G_{yr}^p(j\omega)|$.

performance loss, we approximate $G_{yr}(s)$ with k tuned according to Equation (28) by obtaining Equation (29):

$$G_{yr}^p(s) \triangleq \left(\frac{\rho_\omega \omega_c}{s + \rho_\omega \omega_c} \right)^2, \quad (29)$$

while the ideal case in Equation (24) is re-written as given by Equation (30):

$$G_{yr}^\infty(s) \triangleq \left(\frac{\omega_c}{s + \omega_c} \right)^2. \quad (30)$$

It follows from algebraic computations that the error between $G_{yr}^\infty(s)$ and $G_{yr}^p(s)$ is given by Equation (31):

$$\begin{aligned} E_1(\omega) &\triangleq \left| |G_{yr}^p(j\omega)| - |G_{yr}^\infty(j\omega)| \right| \\ &\leq \max_\omega \left| |G_{yr}^p(j\omega)| - |G_{yr}^\infty(j\omega)| \right| = \frac{1 - \rho_\omega}{1 + \rho_\omega}. \end{aligned} \quad (31)$$

If $\rho_\omega = 0.9$, then $E_1(\omega) \leq 0.0526$, which is less than 10%. Note that $E_2(\omega) \triangleq \left| |G_{yr}(j\omega)| - |G_{yr}^p(j\omega)| \right|$ is small in contrast with $E_1(\omega)$. For example, consider Equation (27) with a specification of $\rho_\omega = 0.9$ and a tuned gain of $k = 15.1$, it can be seen from Figure 5 that $E_2(\omega)$ is very small. Since $E(\omega) \leq E_1(\omega) + E_2(\omega)$, it is concluded that the error bound for $E_1(\omega)$ in Equation (31) dominates $E(\omega)$. Hence, the above formula approximately gives the performance loss (E) in terms of frequency response magnitude when a finite gain of k is used. Note that this bound is independent of ω_c or other frequencies.

Internal stability

Suppose that a system with scalar signals has n subsystems, $g_i(s)$, $i = 1, 2, \dots, n$ and $p_i(s)$ is the characteristic polynomial of $g_i(s)$. Define the closed-loop characteristic polynomial as

$$p_c(s) = \Delta \prod_{i=1}^n (p_i(s)).$$

Proposition 1 (Wang et al., 1999b). A linear time-invariant interconnected system with scalar signals is internally stable if

and only if $p_c(s)$ has all its roots in the open left half of the complex plane.

We apply Proposition 1 to the system in Figure 1. The overall system has four subsystems with dynamics whose characteristic polynomials are $a(s)$ for the plant, $(s + k)$ for $D(s)$, $(s + k)$ for $D(s)$, and $(s + k)^2$ for $H(s)$, respectively. There are four loops as discussed in the preceding section. The closed-loop characteristic polynomial is given by Equation (32):

$$\begin{aligned} p_c(s) &= a(s)(s + k)^4 \\ &\left[1 - H(s) + \frac{G(s)D(s)D(s)}{b_0} + \frac{\alpha_1 G(s)D(s)}{b_0} + \frac{\alpha_0 G(s)}{b_0} \right] \\ &= (s + k)^4 \left[a(s)s(s + 2k) + k^2 s^2 + \alpha_1 ks(s + k) + \alpha_0 (s + k)^2 \right]. \end{aligned} \quad (32)$$

The factor of $p_{c1}(s) \triangleq (s + k)^2$ acts like the observer polynomial which is stable for any $k > 0$. Thus, $p_c(s)$ is stable if and only if

$$p_{c2}(s) = a(s)s(s + 2k) + k^2 s^2 + \alpha_1 ks(s + k) + \alpha_0 (s + k)^2,$$

is stable.

The perturbation analysis is carried out as follows to determine the root distribution of $p_{c2}(s)$ when k tends to infinity. Let $\varepsilon = 1/k > 0$ and consider the resulting Equation (33):

$$\varepsilon^2 s^2 [a(s) + \alpha_0] + \varepsilon s [2a(s) + \alpha_1 s + 2\alpha_0] + \alpha(s) = 0, \quad (33)$$

where $\alpha(s) \triangleq s^2 + \alpha_1 s + \alpha_0 = (s + \omega_c)^2$ is the previously defined desired closed-loop characteristic polynomial. In the limiting case of $\varepsilon \rightarrow 0$, the quartic equation degenerates to a quadratic one, $\alpha(s) = 0$, with the desired solutions at $-\omega_c$ that could be specified by the user. Substituting a regular perturbation series, Equation (34):

$$s(\varepsilon) = s_0 + s_1 \varepsilon + s_2 \varepsilon^2 + \dots, \quad (34)$$

into Equation (33) and equalizing the coefficients of the same powers of ε on both sides yields

$$s_0 = -\omega_c, s_1 = -s_0(a_0 + \alpha_0)/(2s_0 + \alpha_1 + 2\alpha_1 s_0), \dots$$

The solution series approaches the stable ones at $-\omega_c$, and thus there exists $\varepsilon = \varepsilon_1 > 0$ such that these two finite roots of $p_{c2}(s)$ are in the left half plane for $\varepsilon < \varepsilon_1$, or $k > k_1 \triangleq 1/\varepsilon_1$.

The other two roots of $p_{c2}(s)$ could be found by singular perturbation analysis. To track these two roots which may escape to infinity when $\varepsilon \rightarrow 0$, we define a rescaled variable, $s = z/(\varepsilon)^q$. Substituting z into Equation (33) yields Equation (35):

$$\begin{aligned} &z^4 + (a_1 \varepsilon^q + 2\varepsilon^{q-1})z^3 \\ &+ [(a_0 + \alpha_0)\varepsilon^{2q} + (2a_1 + \alpha_1)\varepsilon^{2q-1} + \varepsilon^{2q-2}]z^2 \\ &+ [(2a_0 + 2\alpha_0)\varepsilon^{3q-1} + \alpha_1 \varepsilon^{3q-2}]z + \alpha_0 \varepsilon^{4q-2} = 0. \end{aligned} \quad (35)$$

Setting $q = 1$ gives rise to Equation (36):

$$z^4 + (a_1\varepsilon + 2)z^3 + [(a_0 + \alpha_0)\varepsilon^2 + (2a_1 + \alpha_1)\varepsilon + 1]z^2 + [(2a_0 + 2\alpha_0)\varepsilon^2 + \alpha_1\varepsilon]z + \alpha_0\varepsilon^2 = 0. \quad (36)$$

Letting a singular perturbation series be $z(\varepsilon) = z_0 + z_1\varepsilon + z_2\varepsilon^2 + \dots$ and equalizing the coefficients of zero power of ε on both sides of Equation (36) yields Equation (37):

$$(z_0^2 + 2z_0 + 1)z_0^2 = 0. \quad (37)$$

Its two solutions at the origin correspond to what has been found before from regular perturbation: they are finite in the origin scale (s) but collapse to zero in the limit of the re-scaled z . We are only interested in the other two solutions of Equation (37) located at $z_0 = -1$. Computing the first few terms in the series $z(\varepsilon)$ and recovering the original scale x yield the other two solutions of Equation (33) as

$$s(\varepsilon) = \frac{z_0}{\varepsilon} + z_1 + z_2\varepsilon + \dots$$

Such a solution series approaches the stable one at $z_0/\varepsilon = -1/\varepsilon$, and thus there exists $\varepsilon = \varepsilon_2 > 0$ such that these two roots are also in the left half plane for $\varepsilon < \varepsilon_2$.

In view of the above analysis, all the four solutions of Equation (33) are in the left half plane for $\varepsilon < \varepsilon^* \triangleq \min(\varepsilon_1, \varepsilon_2)$. Equivalently, all the four roots of Equation (32) are in the left half plane for $k > k^* \triangleq 1/\varepsilon^*$. We thus have the following theorem.

Theorem 1. The system in Figure 1 is internally stable if $p_c(s)$ in Equation (32) is a stable polynomial. Specifically, there is a $k^* > 0$ such that the system is internally stable for all $k > k^*$.

The exact gain intervals of k for closed-loop stability can be determined by the D-decomposition method (Le et al., 2015), which is illustrated as follows.

Example 1. Consider the stable plant in Equation (27) with $a(s) = s^2 + 2s + 3$. Set the desired closed-loop characteristic polynomial $\alpha(s) = s^2 + 4s + 4$ in (6). We have

$$\begin{aligned} p_{c2}(s) &= a(s)s(s + 2k) + k^2s^2 + \alpha_1ks(s + k) + \alpha_0(s + k)^2 \\ &= s^4 + (2k + 2)s^3 + (k^2 + 8k + 7)s^2 + (4k^2 + 14k)s + 4k^2. \end{aligned}$$

Let $s = j\omega$. Separating the real and imaginary parts give a pair of equations:

$$\begin{aligned} \omega^4 - (k^2 + 8k + 7)\omega^2 + 4k^2 &= 0, \\ -(2k + 2)\omega^3 + (4k^2 + 14k)\omega &= 0. \end{aligned}$$

Their solutions, (ω, k) , are computed numerically, which is unique at $k = 0$. The solution divides real k to two intervals: $k < 0$ and $k > 0$. Taking one point in each interval, one easily finds that the system is unstable for $k = -1$ but stable for $k = 1$. It is therefore concluded that the system is stable only for $k > 0$. The root loci with regards to $k > 0$ are computed and shown in Figure 6, demonstrating that all the roots are in the left half plane. The interval of k for the closed-loop stability is very large with $k > k^* = 0$.

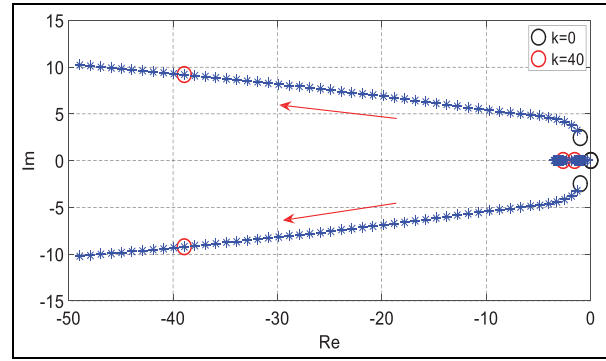


Figure 6. Root locus for Example 1.

The design procedure is summarized as follows:

Step 1: specify ω_c for the desired closed-loop model Equation (5);

Step 2: conduct stability analysis by Theorem 1 to determine the stabilizing gain interval, (k^*, ∞) ; and

Step 3: select a suitable estimator gain k with the transient analysis with a finite gain $k > k^*$ by specifying ρ_g in Equation (26) or ρ_w in Equation (28).

Remark 2: In its discrete time version, our new scheme will predict future output in two steps ahead instead of \ddot{y} . It should be pointed out that in this era of big data, huge data are available and data mining techniques have evolved to high standards with wide successful applications. And this trend is likely to continue or even accelerate. Therefore, it is expected that the prediction-based schemes will have huge potentials for technical development and practical applications.

Simulation examples

Example 2. Consider the following stable plant with a zero,

$$G(s) = \frac{5s + 1}{50s^2 + 12s + 1}.$$

There are a unit step change in the reference r at $t = 0$ (s) and a step disturbance at $t = 50$ (s), $w(t) = -10 \cdot 1(t - 50)$. To make a fair comparison with the ESO/ADRC method (Gao, 2006, 2014), we take $b_0 = 0.02$ and $k = 2$ for the proposed scheme, while $b_0 = 0.02$ and $\omega_0 = 2$ are used for ADRC according to the guidelines given therein, so that both have the same desired estimation dynamics. Furthermore, both schemes are designed with the state feedback to achieve the same target closed-loop characteristic polynomial with $\omega_c = 0.5$. The simulation results are given in Figure 7. It is seen that while the reference tracking performance is similar, an obvious improvement on DR is obtained with the proposed method, owing to: (a) the guaranteed uncertainty estimation transient as discussed in the third section, which does

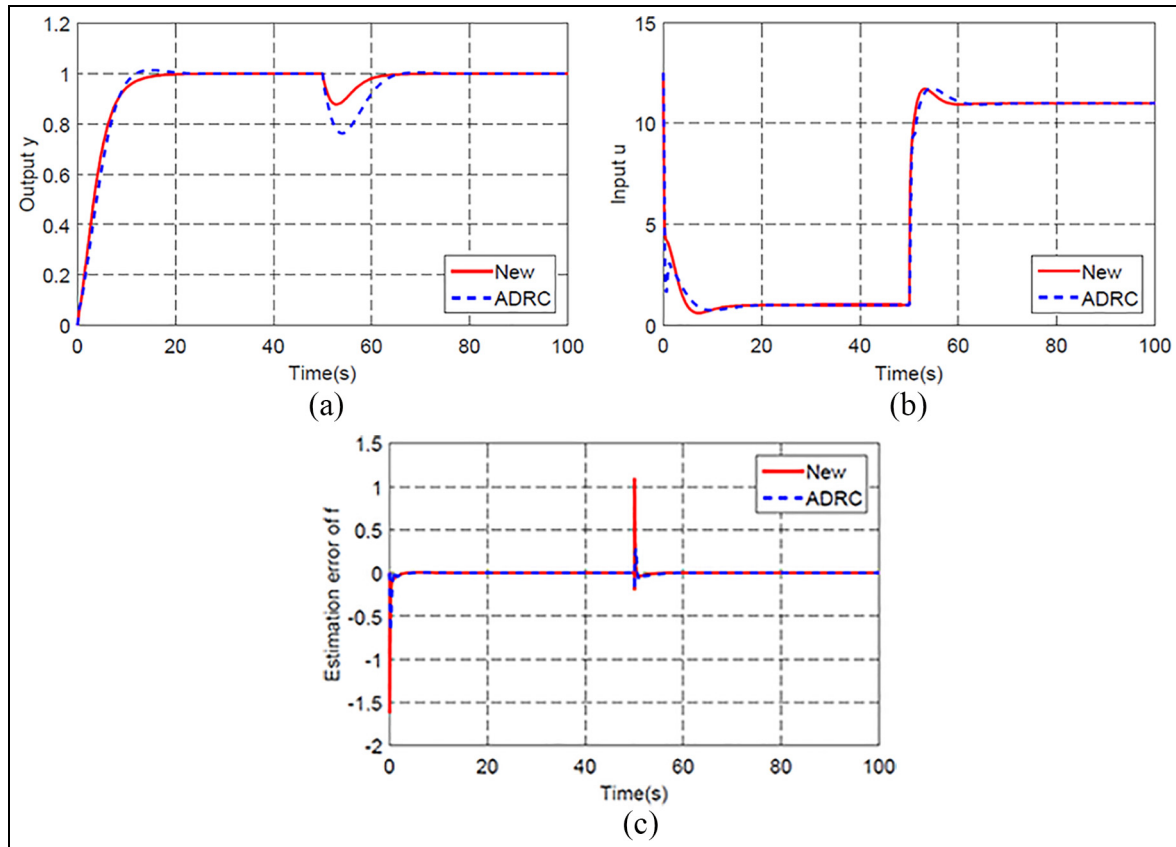


Figure 7. Nominal response for Example 2.

not exist for ADRC; and (b) lower-order estimation, that is, the second-order of the estimator-controller compared with the third-order of the observer-controller of ADRC with an extended state variable, therefore leading to faster dynamics based on the same closed-loop system poles.

To test the robustness in the presence of modelling error, suppose that the plant gain, b_0 , is actually 50% smaller than that of the model used in the control design. Figure 8 shows the simulation results. It is seen that the proposed method well maintains robust stability in contrast with ADRC.

To demonstrate the robustness in the presence of measurement noise, the output is corrupted by white noise $n(t)$ with the noise-to-signal ratio of 10%, as shown in Figure 1. With the noisy output, a low-pass filter $L_f(s)$ in Figure 1 is taken in the form of

$$L_f(s) = \frac{1}{\eta s + 1},$$

where η is a tuning parameter, which in this case is set as $\eta = 0.3$. The others are identical with the above design. The control results are depicted in Figure 9. It is seen that the output response remains almost the same as the nominal case, except for minor high-frequency fluctuations due to noise, which occur in both designs.

Example 3. Consider the following unstable and nonlinear plant (Huang and Xue, 2014; Nie et al., 2020) with

$$\begin{cases} \dot{x}_{p1}(t) = x_{p2}(t) \\ \dot{x}_{p2}(t) = f(x_{p1}, x_{p2}, d, t) + b_0 u(t) \\ y(t) = x_{p1}(t) \end{cases}$$

where $f(x_{p1}, x_{p2}, d, t) = 8\sin(80x_{p1} + 0.01\pi) + 10x_{p2} + w(t)$ is the unknown total disturbance, $w(t) = 10^3 \cdot 1(t - 2.5)$ is the external disturbance and the input gain is $b_0 = 1.5$. There is a step change in the reference $r = 10 \cdot 1(t)$ and a disturbance $w(t)$ at $t = 10s$. To make a fair comparison with the recently developed ADRC method (Tan and Fu, 2016), we take $\omega_c = 10$, $b_0 = 1.5$ and $k = 100$ for the proposed scheme, and $\omega_c = 10$, $b_0 = 1.5$ and $\omega_o = 100$ for ADRC (Tan and Fu, 2016) according to the guidelines given therein. The control results are shown in Figure 10. It is again seen that obviously better DR is obtained with the proposed scheme.

Suppose that the process gain is actually 50% larger than that of the model used in the controller design. The perturbed system response is shown in Figure 11. It is once again seen that the proposed method well maintains the control robustness and system stability.

Experimental verification

Consider an electrical signal amplifier made by Tsinghua Ltd. (product no. XMN-2) with a control computer, as shown in Figure 12. This plant has an integral function to amplify the magnitude of the input signal while maintaining the signal frequency. The main components include a complementary

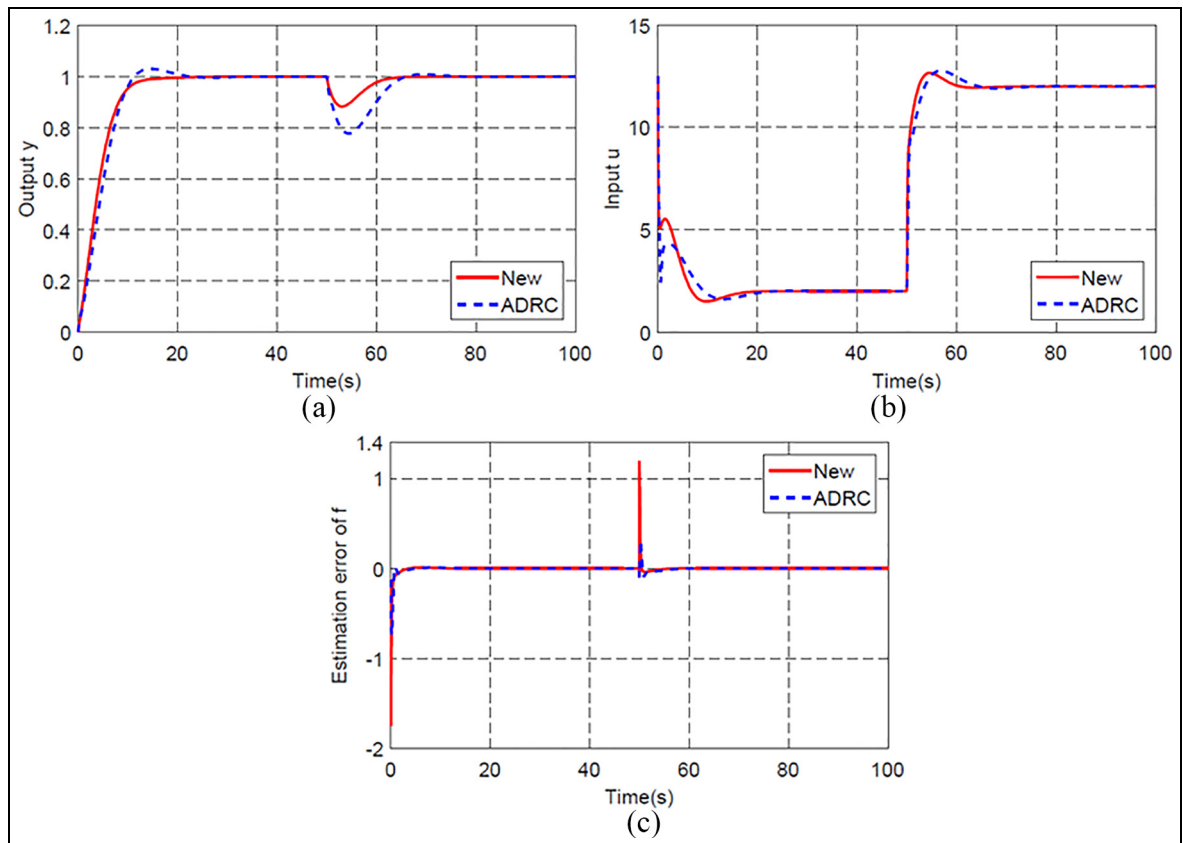


Figure 8. Perturbed response for Example 2.

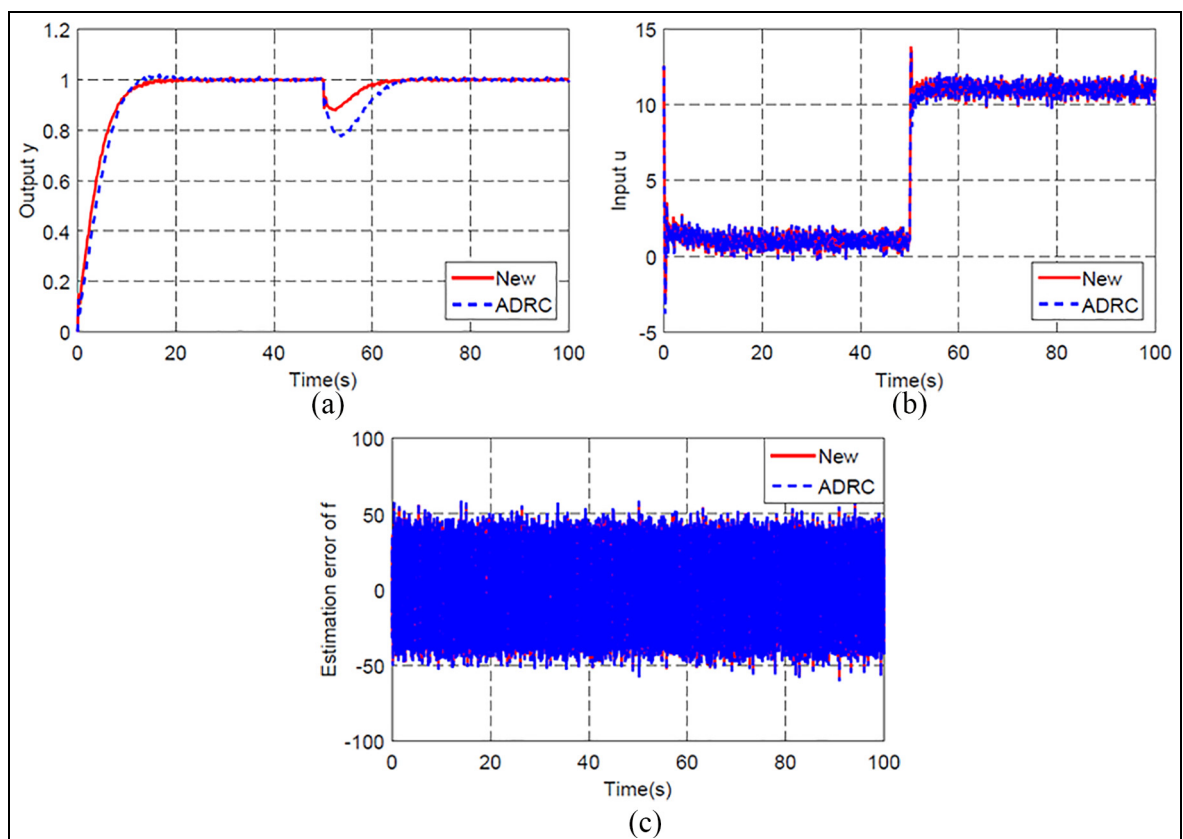


Figure 9. System response under measurement noise for Example 2.

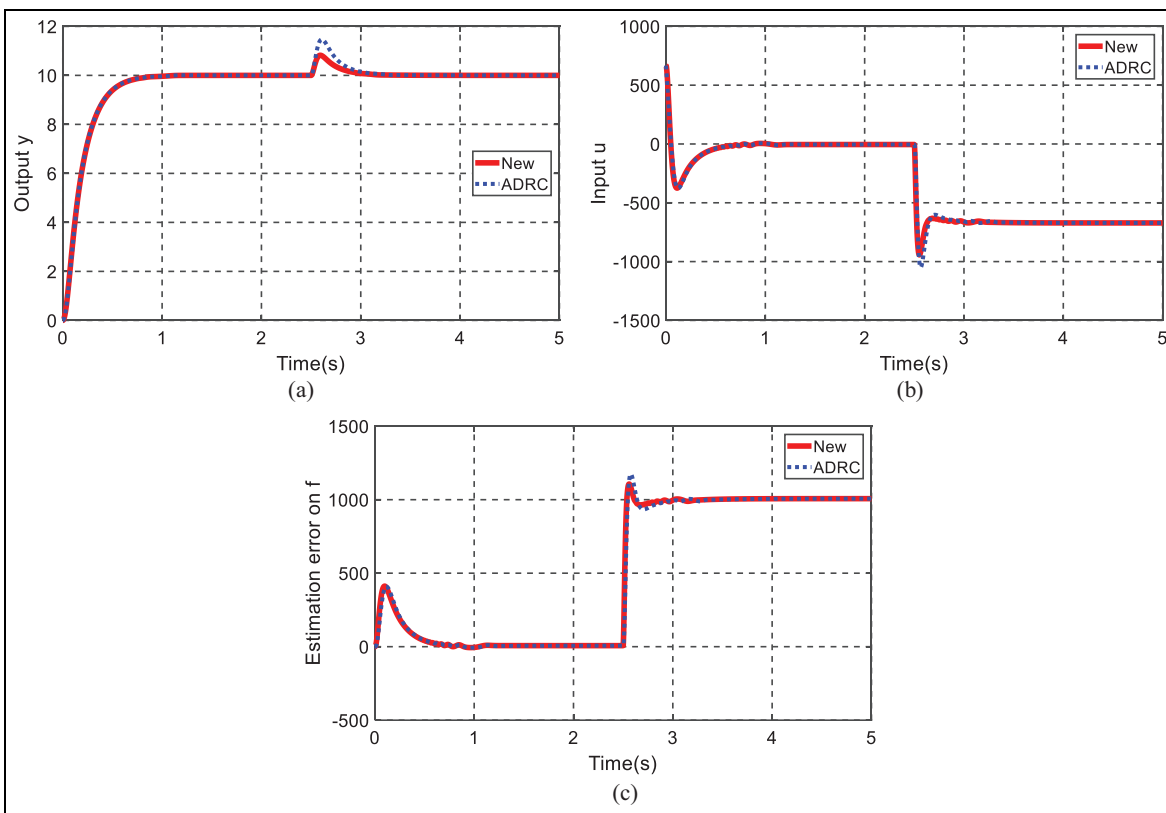


Figure 10. Nominal response for Example 3.

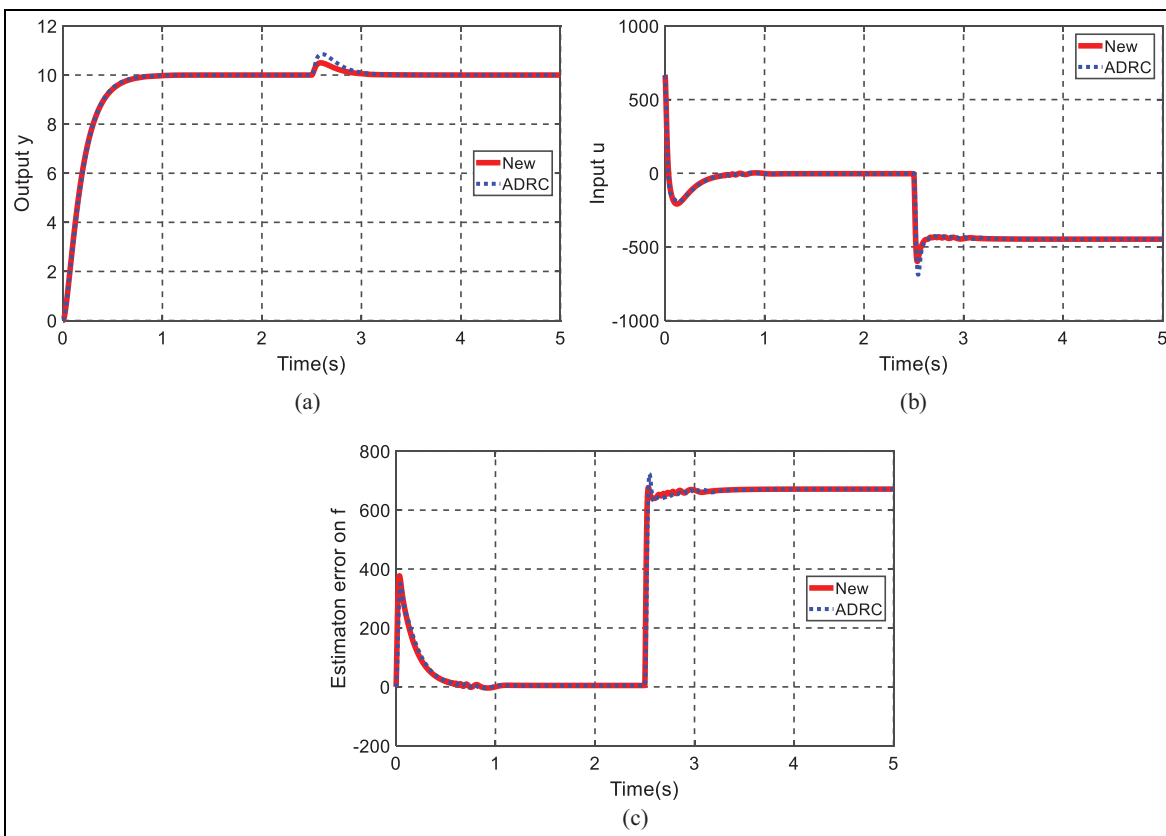


Figure 11. Perturbed response for Example 3.

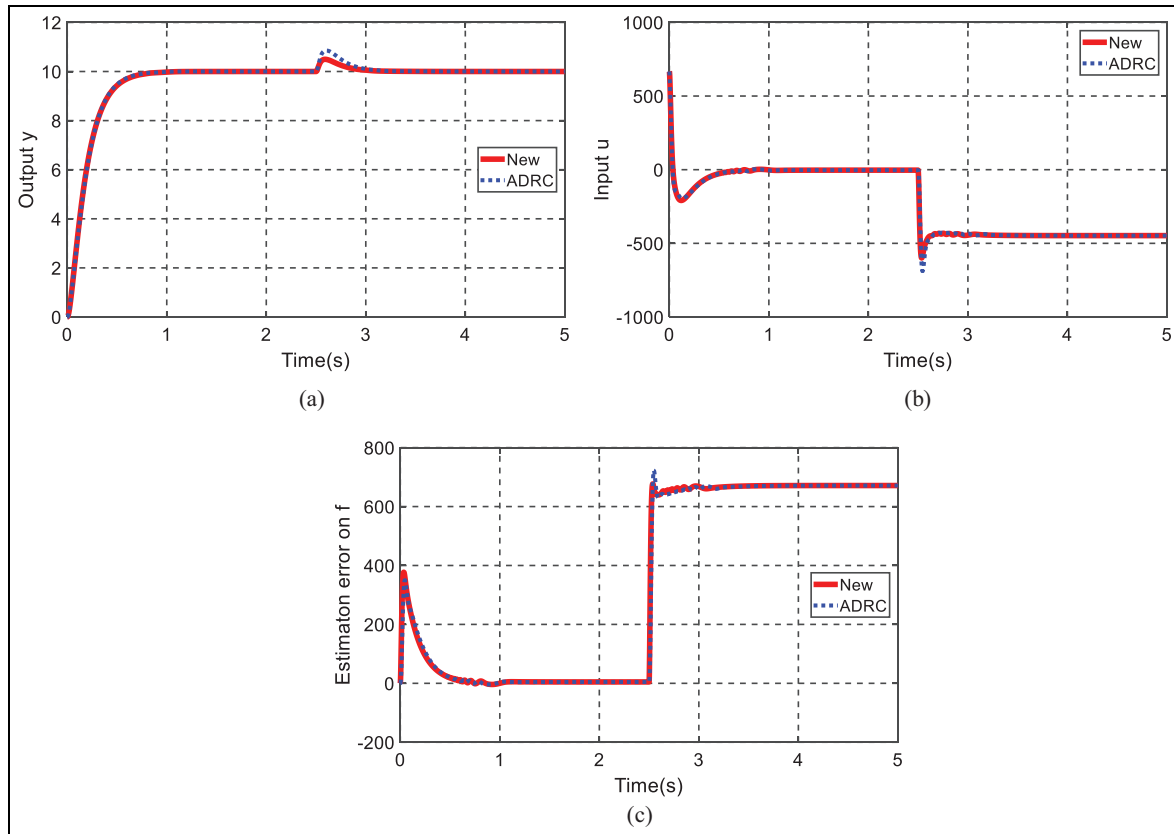


Figure 12. Experimental set up.

metal–oxide–semiconductor operational amplifier (OP07) with a gain range of $[0, 10]$, a resistor–capacitor unit of integral function with $R = 2.5(m\Omega)$ and $C = 8(\mu F)$, and an alternating current power source of 50W. A 32-bit data acquisition card made by TAIDI Ltd (product no. PCI2013) is used for analogue-to-digital and digital-to-analogue conversions.

To amplify a sinusoidal signal with amplitude $A_0 = 0.5$ and frequency 0.025Hz to the amplitude $A_m = 2$ along with the same frequency, the transfer function of the signal amplifier was configured as

$$G(s) = \frac{5}{s(5s + 1)}.$$

To perform an experimental test under a load disturbance, a square wave type disturbance with a magnitude of -5 and width of 10 seconds is added to the amplifier input at $t = 50$ s. For a fair comparison, we take $\omega_c = 2$, $b_0 = 1$ and $k = 5$ in the proposed control scheme, and $\omega_c = 2$, $b_0 = 1$, and $\omega_0 = 5$ for the recently developed ADRC method (Tan and Fu, 2016) according to the guidelines given therein. The experiment was conducted on each scheme, respectively. The control results are shown in Figure 13. It is seen that the proposed method well tracks the reference signal, while the DR performance is evidently improved with respect to both the disturbance response peak and recovering time, compared with the ADRC method (Tan and Fu, 2016).

Conclusions

A novel control scheme has been developed in this paper for a continuous-time system with possibly large uncertainty arising from unknown internal dynamics or external disturbances. The output derivatives are estimated by realizable differentiators with finite gains so as to track and cancel the uncertainty faster than ESO. The new scheme enables rigorous analysis of the system with a finite gain, which is not addressed in the literature on ESO or other control schemes. In particular, the estimation transient is analysed for the proposed scheme with a finite estimator gain and the precise error formulae are obtained. The control performance associated with realizable gains is quantified by tight bounds with respect to the ideal case. The necessary and sufficient condition for the internal stability of the control system is established, along with a D-decomposition method to determine the complete set of the gain intervals which could internally stabilize the plant. Finally, the proposed scheme has been tested via simulation examples and an electrical signal amplifier. The results demonstrate significant improvement on DR performance over the well-recognized ADRC method. The future research directions include, but are not limited to the extension of the proposed scheme to time delay systems, internal stability analysis of nonlinear systems of the scheme, robust design and stability analysis for plant order uncertainties, control performance design and analysis with input constraint, and better ways to approximate differentiators.

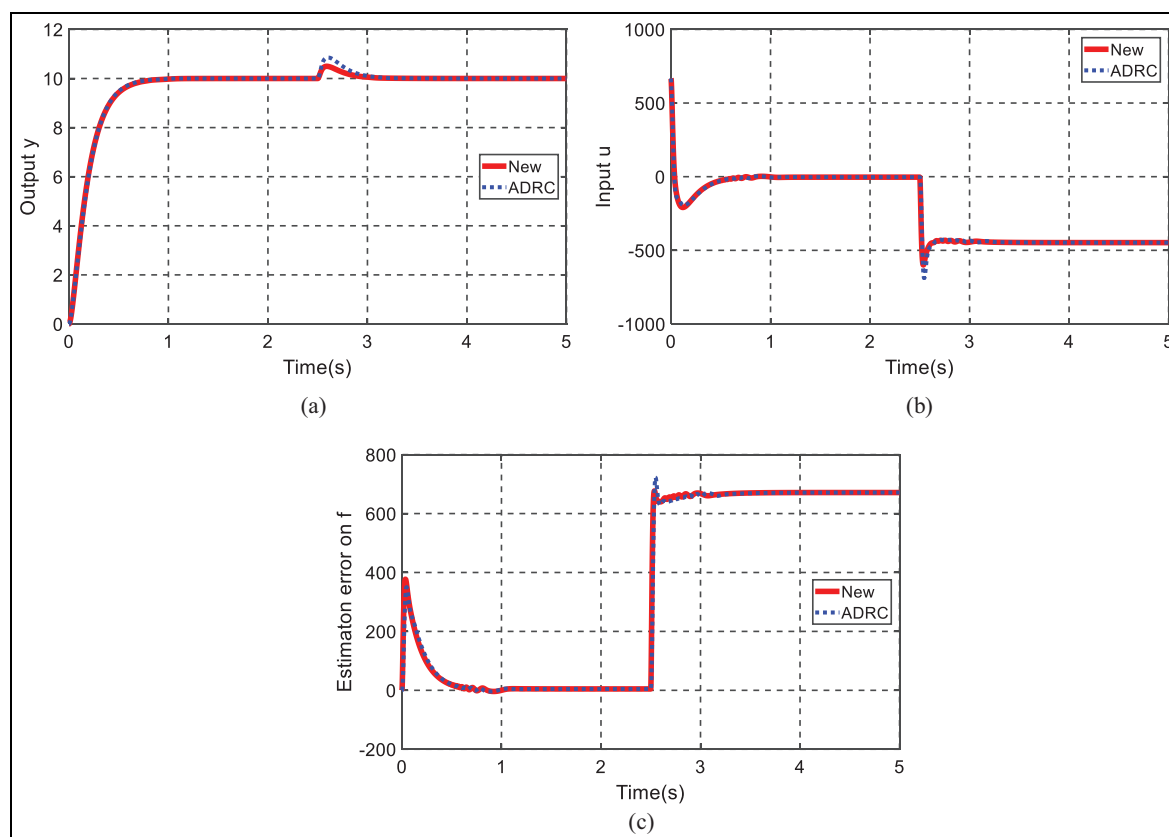


Figure 13. Experimental results.

Declaration of conflicting interests


The authors declared no potential conflicts of interest with respect to the research, authorship, and/or publication of this article.

Funding

The authors disclosed receipt of the following financial support for the research, authorship, and/or publication of this article: Fundamental Research Funds for the Provincial Universities of Zhejiang (Grant Number: RF-A2019003).

ORCID iDs

Zhuo-Yun Nie  <https://orcid.org/0000-0002-5980-3268>

Dan Zhang  <https://orcid.org/0000-0002-1183-2166>

References

- Astrom KJ and Wittenmark B (1994) *Adaptive Control*. Boston: Addison-Wesley.
- Chen W-H, Yang J, Guo L, et al. (2016) Disturbance-observer-based control and related methods—An overview. *IEEE Transactions on Industrial Electronics* 63(2): 1083–1095.
- Chen Z, Sun M and Yang R (2013) On the stability of linear active disturbance rejection control. *Acta Automatica Sinica* 39: 574–580.
- Franklin GF, Powell JD and Emami-Naeini A (2014) *Feedback Control of Dynamic Systems*. 7th edition. Upper Saddle River: Pearson Education.
- Gao Z (2006) Active disturbance rejection control: A paradigm shift in feedback control system design. In: *Proceedings of the American Control Conference*, Minneapolis, Minnesota, USA, 14–16 June 2006. Piscataway, NJ: Institute of Electrical and Electronics Engineers, 2399–2405.
- Gao Z (2014) On the centrality of disturbance rejection in automatic control. *ISA Transactions* 53(4): 850–857.
- Ge SS and Tee K-P (2006) Adaptive neural network control of helicopters. In: Wang J, Yi Z, Zurada JM, et al. (eds) *Advances in Neural Networks – ISNN 2006*. Berlin: Springer, 82–87.
- Guo B-Z and Zhao Z-L (2011a) On convergence of tracking differentiator. *International Journal of Control* 84(4): 693–701.
- Guo B-Z and Zhao Z-L (2011b) On the convergence of an extended state observer for nonlinear systems with uncertainty. *Systems & Control Letters* 60(6): 420–430.
- Guo B-Z and Zhao Z-L (2012) On convergence of non-linear extended state observer for multi-input multi-output systems with uncertainty. *IET Control Theory and Applications* 6(15): 2375–2386.
- Han J (2009) From PID to active disturbance rejection control. *IEEE Transactions on Industrial Electronics* 56(3): 900–906.
- Hao S, Liu T and Zhou B (2017) Predictor-based output feedback control design for sampled systems with input delay subject to disturbance. *IET Control Theory and Applications* 11(18): 3329–3340.
- He J-B, Wang Q-G and Lee T-H (2000) PI/PID controller tuning via LQR approach. *Chemical Engineering Science* 55: 2429–2439.

- Huang Y and Xue W (2014) Active disturbance rejection control: Methodology and theoretical analysis. *ISA Transactions* 53(4): 963–976.
- Le BN, Wang Q-G and Lee T-H (2015) Development of D-decomposition method for computing stabilizing gain ranges for general delay systems. *Journal of Process Control* 25: 94–104.
- Li S, Yang J, Chen W-H, et al. (2012) Generalized extended state observer-based control for systems with mismatched uncertainties. *IEEE Transactions on Industrial Electronics* 59(12): 4792–4802.
- Li Y, Sun M, Wang Z, et al. (2016) Quantitative analysis of critical limitation in using extended state observer. *International Journal of Control, Automation and Systems* 14: 876–882.
- Liu H and Li S (2011) Speed control for PMSM servo system using predictive functional control and extended state observer. *IEEE Transactions on Industrial Electronics* 59(2): 1171–1183.
- Liu T, Hao S, Li D, et al. (2017) Predictor-based disturbance rejection control for sampled systems with input delay. *IEEE Transactions on Control Systems Technology* 27(2): 772–780.
- Liu W, Zhao T, Wu Z, et al. (2020) Linear active disturbance rejection control for hysteresis compensation based on backpropagation neural networks adaptive control. *Transactions of the Institute of Measurement and Control* 43(4): 915–924.
- Mao J, Yang J, Li S, et al. (2018) Output feedback-based sliding mode control for disturbed motion control systems via a high-order ESO approach. *IET Control Theory and Applications* 12(15): 2118–2126.
- Nie Z, Ma Y, Liu R, et al. (2018) Improved disturbance rejection control for piezoelectric actuators based on combination of ESO and Q-filter. *Electronics Letters* 54(14): 872–874.
- Nie Z, Zhang B, Wang Q, et al. (2020) Adaptive active disturbance rejection control guaranteeing uniformly ultimate boundedness and simplicity. *International Journal of Robust and Nonlinear Control* 30(17): 7278–7294.
- Salgado I, Mera-Hernández M and Chairez I (2017) Quasi-minimal active disturbance rejection control of MIMO perturbed linear systems based on differential neural networks and the attractive ellipsoid method. *ISA Transactions* 71(2): 304–316.
- Sheng Y, Bai W and Xie Y (2021) Fractional-order PI λ D sliding mode control for hypersonic vehicles with neural network disturbance compensator. *Nonlinear Dynamics* 103: 849–863.
- Sun L, Li D, Gao Z, et al. (2016) Combined feedforward and model-assisted active disturbance rejection control for non-minimum phase system. *ISA Transactions* 64: 24–33.
- Sun L, Li G and You F (2020) Combined internal resistance and state-of-charge estimation of lithium-ion battery based on extended state observer. *Renewable and Sustainable Energy Reviews* 131: 109994.
- Tan W and Fu C (2016) Linear active disturbance-rejection control: Analysis and tuning via IMC. *IEEE Transactions on Industrial Electronics* 63(4): 2350–2359.
- Wang J, Li S, Yang J, et al. (2015) Extended state observer-based sliding mode control for PWM-based DC–DC buck power converter systems with mismatched disturbances. *IET Control Theory and Applications* 9(4): 579–586.
- Wang Q-G, Lee T-H, Fung H-W, et al. (1999a) PID tuning for improved performance. *IEEE Transactions on Control Systems Technology* 7(4): 457–465.
- Wang Q-G, Lee T-H and He J-B (1999b) Internal stability of interconnected systems. *IEEE Transactions on Automatic Control* 44(3): 593–596.
- Wang Z, Hu C, Zhu Y, et al. (2017) Neural network learning adaptive robust control of an industrial linear motor driven stage with disturbance rejection ability. *IEEE Transactions on Industrial Informatics* 13(5): 2172–2183.
- Xue W, Bai W, Yang S, et al. (2015) ADRC with adaptive extended state observer and its application to air–fuel ratio control in gasoline engines. *IEEE Transactions on Industrial Electronics* 62(9): 5847–5857.
- Yao J, Jiao Z and Ma D (2014) Adaptive robust control of DC motors with extended state observer. *IEEE Transactions on Industrial Electronics* 61(7): 3630–3637.
- Zhang Y, Wang Q-G and Astrom KJ (2002) Dominant pole placement for multi-loop control systems. *Automatica* 38(7): 1213–1220.
- Zhao Z-L and Guo B-Z (2017) A nonlinear extended state observer based on fractional power functions. *Automatica* 81, 286–296.
- Zheng Q, Gao L and Gao Z (2012) On validation of extended state observer through analysis and experimentation. *Journal of Dynamic Systems, Measurement, and Control* 134(2): 024505.